JOURNAL OF SOLID STATE CHEMISTRY 115, 447–455 (1995)

High Oxygen Pressure and the Preparation of New Iridium (VI) Oxides with Perovskite Structure: Sr_2MIrO_6 (M = Ca, Mg)[1]

Duk-Young Jung and Gérard Demazeau[2]

Laboratoire de Chimie du Solide du CNRS and Interface Hautes Pressions, LCS-CNRS/ENSCPB, Université de Bordeaux I, 33405 Talence Cedex, France

Received January 14, 1994; in revised form July 25, 1994; accepted July 28, 1994

Ir(VI) in an octahedral coordination has been stabilized in Sr_2MIrO_6 (M = Ca, Mg) oxides with an ordered perovskite structure by use of high oxygen pressure. The structure of Sr_2CaIrO_6 depends strongly on the oxygen pressure and reversibly returns to the original structure according to the heat treatment applied. The oxidation state of iridium in each compound is determined by chemical titration and is correlated with the structural factors and the covalency of M–O bonds. The $t_{2g}^3e_g^0$ electronic configuration of Ir(VI) leads to a high Néel temperature with 55 K (M = Ca) and 80 K (M = Mg). The samples are not metallic conductors. © 1995 Academic Press, Inc.

INTRODUCTION

Alkali metal ternary oxides of iridium have been prepared and characterized during the past 20 years (1–22). In the majority of iridium compounds Ir(IV) is stablized. Ir(V) was prepared in the double-perovskites La_2LiIrO_6 (23–25) and ALaMgIrO$_6$ (A = Ca, Sr, and Ba) (26) using oxygen pressures (27).

Twenty years ago, Sleight first reported the pyrochlore oxides containing Ir(V) (9). Also Ir(V) was stabilized in the perovskite oxides Ba_2BIrO_6 (B = La, Nd, Sm, Gd, Dy, Y, In, Er) and $Ba_3B'Ir_2O_9$ (B' = Mg, Ni, Zn, Co, Fe, Cd) (28–35).

Recently we have reported the +6 oxidation state of iridium in the perovskite lattice Ba_2MIrO_6 (M = Ca, Sr) (36–37). Ca_3IrO_6 is the only Ir(VI) oxide reported previously, but the publication is inaccessible and preparative details are unknown (38).

Due to its position in the Periodic Table and the highest value of the oxidation state +6, the Ir(VI)–O bond could be one of the strongest chemical bonds in an oxygen lattice. The purpose of this work is to evaluate the influence of the covalency of such chemical bonding on the values of the Néel temperature versus the size of the 12-coordinated (A) and 6-coordinated (M) cations in the A_2MIr(VI)O$_6$ perovskite lattice.

[1] This paper is dedicated to Professor Q. W. Choi (Seoul National University), an initiator of Solid State Chemistry in Korea.

[2] To whom correspondence should be addressed.

EXPERIMENTAL

The stoichiometric reactants, $SrCO_3$, $CaCO_3$, $[4(MgCO_3) \cdot Mg(OH)_2 \cdot 5H_2O]$, and IrO_2 were weighed and mixed thoroughly in an agate mortar. They were placed in a platinum crucible and heated in flowing oxygen in an electric furnace at 950°C for 3 days with frequent grinding. Only the Sr_2CaIrO_6 phase was treated again in 1100°C in air overnight in order to obtain good quality crystallinity. The resulting powder was then heated in a gold tube at 880°C under 600 bar (60 MPa) of oxygen for 48 hr (39).

For the electrical conductivity measurements the pelletized samples were treated again under oxygen pressure (600 bar (60 MPa)) to ensure oxygen stoichiometry.

In order to investigate the influence of the very high oxygen pressures on the stabilization of Ir(VI) the samples with $KClO_3$ (as the *in situ* oxygen source at high temperature) were intimately packed into cylindrical platinum capsules and subjected to high pressure (up to 60 kbar (6 GPa)) in a belt-type apparatus before the temperature was raised (39). After 5 min at 900°C, all samples were quenched, followed by release of pressure.

PHYSICO-CHEMICAL CHARACTERIZATION

Chemical Titration and Thermal Analysis

The determination of the iridium oxidation state of the samples after each experimental step was monitored by chemical titration methods in aqueous solution. The iodometric titration for Sr_2CaIrO_6 and the back-titration method using Mohrs salt for Sr_2MgIrO_6 were developed, respectively, because Sr_2MgIrO_6 is not soluble in weak acidic solutions. The results obtained are given in Table 1. At atmospheric pressure we could not obtain pure irid-

0022-4596/95 $6.00

TABLE 1

Average Iridium Oxidation State (±0.05) Determined by Redox Titration and Proposed Chemical Formulas for Sr_2MIrO_6 (M = Ca, Mg) Oxides

Experimental conditions	Sr_2CaIrO_6	Sr_2MgIrO_6
950°C (or 1100°C)	Ir(+5.38)	Ir(+5.29)
1 bar, 72 hr	$Sr_2CaIrO_{5.69}$	$Sr_2MgIrO_{5.65}$
880°C	Ir(+5.98)	Ir(+5.75)
600 bar (60 MPa), 48 hr	$Sr_2CaIrO_{5.99}$	$Sr_2MgIrO_{5.88}$
900°C	Ir(+5.98)	Ir(+5.81)
60 kbar (6 GPa), 5 min	$Sr_2CaIrO_{5.99}$	$Sr_2MgIrO_{5.91}$

ium (VI) perovskite compounds for the given compositions.

The iridium oxidation state in Sr_2CaIrO_6 is close to the ideal value of 6, after either 600 bar (60 MPa), 880°C heat treatment or after *in situ* decomposition of $KClO_3$ in a belt apparatus.

In order to confirm the oxygen content in Sr_2CaIrO_6, thermogravimetric analysis (TGA) were performed for stoichiometric Sr_2CaIrO_6 with a heating/cooling rate of 4°C/min in air. Three distinct domains of stoichiometry were observed within the temperature range 20–1050°C, as shown in Fig. 1 (the proposed chemical formulas in each temperature domain are noted). $Sr_2CaIrO_{5.99} \cdot xH_2O$ loses a small amount of adsorbed water (x corresponds to less than 0.1 wt%) up to 300°C. Above that temperature, it loses oxygen to yield $Sr_2CaIrO_{5.94}$. Further oxygen evolution commences at about 800°C. At 1050°C the compound has the stoichiometry of $Sr_2CaIrO_{5.70}$, which corresponds to the formula $Sr_2CaIrO_{5.69}$ calculated by chemical titration in Table 1, for the sample of 1100°C, 1 bar heat treatment. During the cooling period, the sample weight does not increase, which shows the Sr_2CaIrO_6 prepared at high oxygen pressures has a larger amount of Ir(VI) than the sample prepared in ambient pressure.

As in the case of Sr_2CaIrO_6, the oxygen content of $Sr_2MgIrO_{6-\delta}$ strongly depends upon the oxygen partial pressure applied in the synthesis. As shown in Table 1, the oxidation state of iridium in Sr_2MgIrO_6 increases notably from 5.29 to 5.81 after high oxygen pressure treatment with the belt-type apparatus. We have attempted to get a higher value for the iridium oxidation state by changing the synthetic conditions. The oxidation state of 5.81 seems the maximum which we could reach for the Sr_2MgIrO_6 phase. Compared to Sr_2CaIrO_6, such a behavior could be due to the competing Mg–O bond being more covalent than the Ca–O bonds. Consequently, the decrease of the local crystal field energy would destablize the oxidation state of iridium (VI).

Structural Characterization

The X-ray powder diffraction data were obtained at room temperature and at high temperature with a Philips PW1050 spectrogoniometer using Cu$K\alpha$ radiation with a graphite diffracted-beam monochromator. Experimental diffraction line angles were corrected using Si as an internal standard (a_0 = 5.4305 Å at 25°C). Unit cell parameters were calculated by least-squares analysis of the X-ray powder diffraction data. For the refinement of the intensity profile the X-ray diffraction data were collected at each 0.02° of 2θ for 40 sec. In order to minimize the orientation effects, the powder was crushed (less than

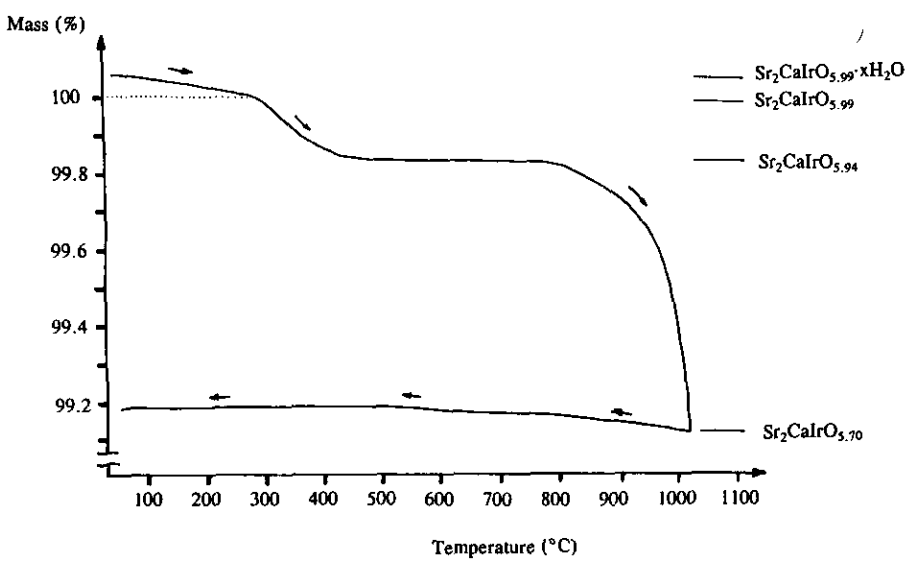

FIG. 1. Oxygen stoichiometry of Sr_2CaIrO_6 versus the heat treatment.

TABLE 2
Structures and Lattice Parameters for Sr_2MIrO_6 (M = Ca, Mg) Oxides by X-ray Powder Diffraction vs the Experimental Conditions (P, T) Used for the Synthesis

Experimental treatment	Sr_2CaIrO_6	Sr_2MgIrO_6
950°C (or 1100°C) 1 bar, 72 hr	Monoclinic structure a = 5.82(1) Å, b = 9.74(1) Å, c = 14.2(1) Å, β = 93(1)°	Cubic perovskite + impurities
880°C 600 bar (60 MPa), 48 hr	Monoclinic perovskite a = 5.7830(2) Å, b = 5.8283(2) Å, c = 8.1997(1) Å, β = 90.26(50)°	Cubic perovskite $a = 2a_0$ = 7.8914(2) Å
900°C 60 kbar (6 GPa), 5 min	Monoclinic perovskite a = 5.78(1) Å, b = 5.83(1) Å, c = 8.20(1) Å, β = 90.2(5)°	Cubic perovskite $a = 2a_0$ = 7.891(1) Å

0.25 μm) and sifted onto the sample holder. The structural analysis is summarized in Table 2.

Sr_2CaIrO_6 prepared at atmospheric pressure could be indexed with a monoclinic unit cell (a = 5.82 Å, b = 9.74 Å, c = 14.2 Å, β = 93°). After the high oxygen pressure treatment the X-ray diffraction pattern changes completely and the structure is transformed to a perovskite with a small distortion. The $GdFeO_3$ structure (40) can be retained. The selected space group was $P2_1/n$ allowing a 1/1 Ir/Ca ordering. Such a space group has been found for ordered perovskites (41, 42). The X-ray diffraction refinement using Rietveld method (43) was accomplished for the stoichiometric Sr_2CaIrO_6, with the program DBW3.2S of Wiles and Young (44).

The converging various parameters are listed in Table 2 for the lattice constants and in Table 3 for the atomic positions. It should be noted that the Bragg-factor R_I drops to 0.045 and the profile factors R_p and R_{wp} are 0.094 and 0.12, respectively. The experimental, calculated, and resulting difference profiles are given in Fig. 2. Table 4 gives the observed and calculated X-ray diffraction patterns.

A high temperature X-ray analysis was carried out in air for the stoichiometric Sr_2CaIrO_6 in order to follow the structural changes. At 500°C the $GdFeO_3$-type structure transforms to a cubic one ($a = 2a_0$ = 8.28(1) Å) and the X-ray pattern does not alter until 1100°C, as shown in Fig. 3, except for the expansion of the cell volume at the high temperature. After 20 min heating at 1100°C and cooling in air, the room temperature pattern shows a small amount of the ambient pressure phase. When the stoichiometric Sr_2CaIrO_6 is heated at 900°C at ambient pressure for 12 hr, it again transforms to the ambient pressure phase completely. The kinetic of such a structural transformation appears not to be fast enough to lead to a complete change during high temperature X-ray analysis. After the loss of oxygen, the cubic perovskite structure transforms to the monoclinic one at ambient pressure.

TABLE 3
Structural Parameters for Sr_2CaIrO_6 Prepared at 880°C and 600 Bar (60 MPa) of Oxygen Pressure (Selected Space Group $P2_1/n$)

Atom	Site	x	y	z	B (Å^2)
Sr	4e	0.0061(5)	0.362(2)	0.2412(4)	0.66(3)
Ca	2d	1/2	0	0	0.35(4)
Ir	2c	1/2	0	1/2	0.34(3)
O1	4e	0.240(2)	0.273(2)	0.030(2)	0.20(11)
O2	4e	0.201(3)	−0.239(2)	0.034(2)	0.20(11)
O3	4e	−0.074(3)	0.432(2)	0.224(2)	0.20(11)

Cubic Sr_2MgIrO_6 is detected in samples prepared at 1 bar. The X-ray spectra are indexed as a cubic perovskite structure with 1/1 Mg/Ir ordering before grinding the calcined sample. After grinding the same sample the X-ray spectra has several weak unindexed peaks, probably $SrIrO_3$ and other impurities, which implies that the formation of the expected perovskite phase occurs only on the surface of the polycrystallites. On the other hand, when we apply the high oxygen pressure (880°C, 600 bar (60 MPa)), the unindexed peaks disappeared completely in the XRD pattern of Sr_2MgIrO_6. High oxygen pressures are required for inducing high iridium (VI) content (5.81 average oxidation state of iridium).

The XRD spectra at two different oxygen pressures (880°C, 600 bar (60 MPa) and 900°C, 60 kbar (6 GPa)) show the same pattern and intensities. Such a result suggests that the Sr_2MgIrO_6 is oxidized during the belt experiment without any change in Mg/Ir ordering in the perovskite lattice. The possibility that the compound has a cubic perovskite structure similar to that of Ba_2CaIrO_6 with the superlattice resulting from the ordering between the six-coordinated cations was examined. However, after comparing the hypothetical intensity calculation for

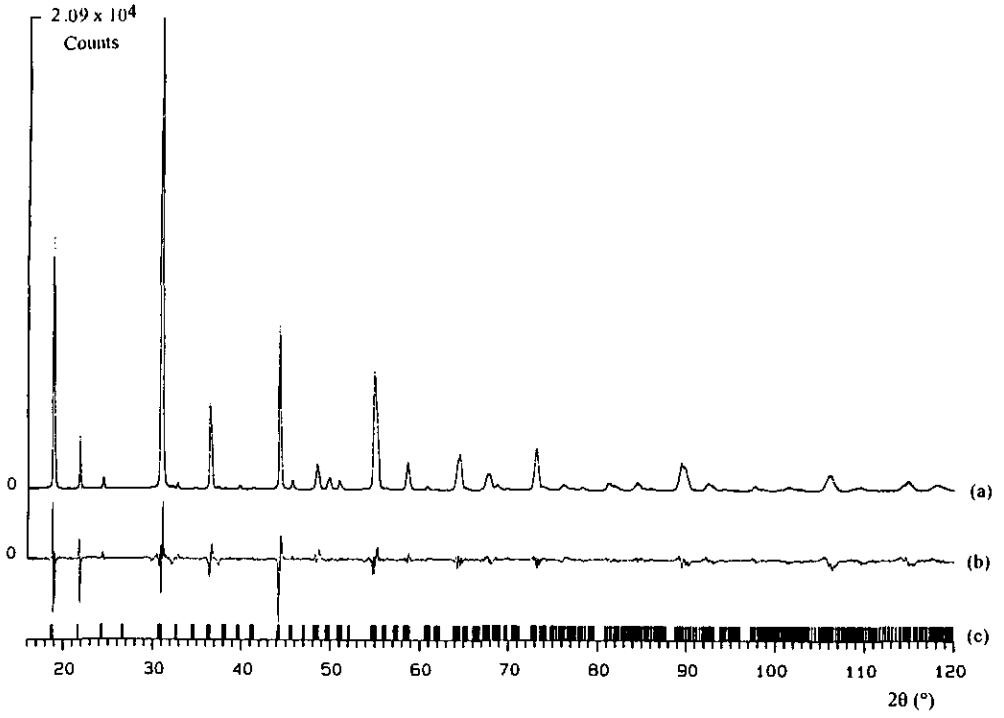

FIG. 2. Rietveld refinement patterns of monoclinic Sr_2CaIrO_6 (after 900°C, 600 bar (60 MPa) treatment) at room temperature: (a) the observed data (dots) and the calculated pattern (solid line) overlap. (b) The difference profile with five times enlargements (c) and the short vertical lines the positions of Bragg reflections.

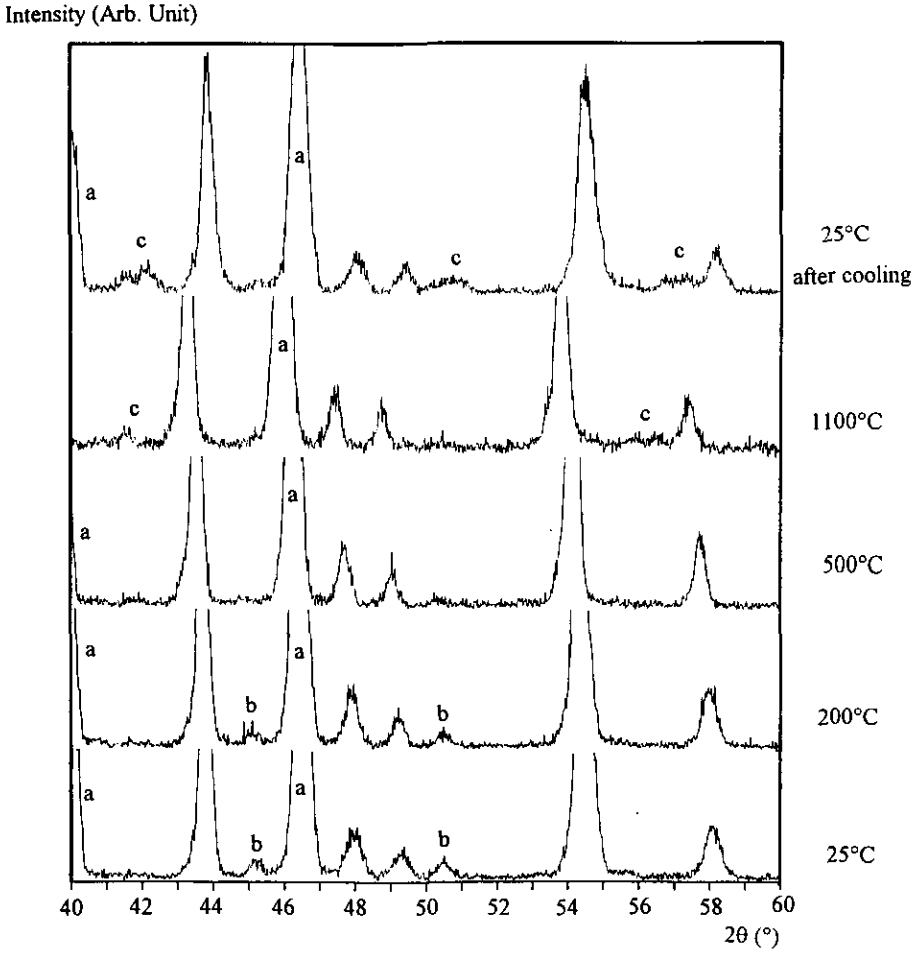

FIG. 3. X-ray diffraction spectra of the stoichiometric Sr_2CaIrO_6 versus the treatment temperature: (a) Pt metal peaks, (b) characteristic peaks of the monoclinic structure of the stoichiometric Sr_2CaIrO_6, and (c) the peaks resulting from the ambient pressure phase.

TABLE 4
Observed and Calculated Powder Diffraction Patterns for Sr_2CaIrO_6 (a = 5.7830(2) Å, b = 5.8283(2) Å, c = 8.1997(1) Å, and β = 90.26(50)°)

h	k	l	I_{calc}	I_{obs}	d_{calc}	d_{obs}	h	k	l	I_{calc}	I_{obs}	d_{calc}	d_{obs}
0	1	−1	16.8		4.751		2	2	2	2.2		1.8330	
0	1	1	16.8	36.4	4.751	4.738	1	1	4	1.1		1.8316	
1	0	−1	37.5		4.736		3	1	0	1.1		1.8302	
1	0	1	33.9		4.716		1	3	−1	3.4		1.7974	
1	1	0	10.2	5.7	4.105	4.104	1	3	1	1.9	2.2	1.7963	1.7974
0	0	2	5.8		4.100		3	1	−1	1.0		1.7887	
1	1	−1	1.5	1.4	3.676	3.670	1	3	−2	17.7		1.6808	
1	1	1	3.2		3.666		1	3	2	17.7		1.6790	
0	2	0	48.4		2.9142		0	2	−4	9.7		1.6766	
1	1	−2	91.0		2.9056		0	2	4	9.7		1.6766	
1	1	2	100.0	100.0	2.8962	2.8954	2	0	−4	12.2	42.1	1.6759	1.6727
2	0	0	50.5		2.8915		3	1	−2	21.1		1.6739	
0	2	−1	1.2	0.8	2.7459	2.7452	2	0	4	8.4		1.6687	
0	2	1	1.2		2.7459		3	1	2	23.8		1.6685	
1	2	0	0.4	0.3	2.6024	2.5936	2	2	−3	0.3	1.4	1.6438	1.6407
2	1	0	0.3		2.5902		2	2	3	0.8		1.6387	
1	2	−1	6.5		2.4819		1	2	4	0.1		1.6087	
1	2	1	11.5		2.4790		3	2	0	0.1	0.1	1.6077	1.6049
1	0	−3	5.5		2.4755		2	1	4	0.1		1.6043	
0	1	−3	4.9	19.0	2.4746	2.4688	0	3	−3	1.6		1.5835	
0	1	3	4.9		2.4746		0	3	3	1.6		1.5835	
2	1	−1	3.7		2.4718		2	3	−1	1.5		1.5830	
2	1	1	14.4		2.4670		2	3	1	3.2		1.5815	
1	0	3	1.0		2.4668		1	0	−5	4.0		1.5796	
0	2	−2	0.1		2.3753		3	2	−1	3.5	8.0	1.5788	1.5764
0	2	2	0.1	0.2	2.3753	2.3743	3	0	−3	0.3		1.5787	
2	0	−2	0.1		2.3680		0	1	−5	0.8		1.5786	
2	0	2	0.1		2.3579		0	1	5	0.8		1.5786	
1	1	−3	1.3	0.7	2.2785	2.2745	3	2	1	3.8		1.5766	
1	1	3	0.7		2.2717		1	0	5	1.8		1.5758	
1	2	−2	0.4		2.1992		3	0	3	0.5		1.5719	
1	2	2	0.4	0.4	2.1951	2.1945	1	3	−3	1.0		1.5283	
2	1	−2	0.1		2.1938		1	3	3	1.6		1.5263	
2	1	2	0.1		2.1853		1	1	−5	0.1	1.0	1.5246	1.5242
2	2	0	53.7	31.1	2.0526	2.0507	1	1	5	0.1		1.5212	
0	0	4	29.9		2.0499		3	1	3	0.3		1.5177	
0	2	−3	1.0		1.9936		2	3	−2	0.1		1.5020	
0	2	3	1.0	1.4	1.9936	1.9910	2	3	2	0.1	0.1	1.4994	1.4847
2	2	−1	2.3		1.9926		3	2	−2	0.1		1.4987	
2	2	1	0.8		1.9896		0	4	0	6.3		1.4571	
0	3	−1	2.5		1.8904		2	2	−4	14.6		1.4528	
0	3	1	2.5		1.8904		2	2	4	15.2		1.4481	
1	2	−3	1.0		1.8867		4	0	0	6.9	15.6	1.4457	1.4463
2	1	−3	7.6		1.8839		0	4	−1	0.7		1.4346	
1	2	3	2.6	7.4	1.8828	1.8786	0	4	1	0.7		1.4346	
3	0	−1	1.0		1.8784		0	2	−5	0.1		1.4292	
2	1	3	3.7		1.8763		0	2	5	0.1		1.4292	
3	0	1	1.7		1.8746		1	4	0	0.2		1.4129	
1	3	0	3.4		1.8416		0	3	−4	0.1	0.1	1.4101	1.4094
2	2	−2	1.1		1.8378		0	3	4	0.1		1.4101	
1	1	−4	1.4	3.7	1.8363	1.8322							

TABLE 5
Observed and Calculated Powder Diffraction Patterns for Sr_2CaIrO_6
Face-Centered Cubic ($Fm3m$), Based on the Unit Cell $a = 2a_0 = 7.8913(2)$ Å

	Relative intensity		Interplanar spacings (Å)	
$h\ k\ l$	I_{obs}	I_{calc}	d_{obs}	d_{calc}
1 1 1	31	45	4.559	4.556
2 0 0	6.4	4.2	3.945	3.946
2 2 0	100	100	2.791	2.790
3 1 1	16	24	2.382	2.379
2 2 2	0.9	1.5	2.278	2.278
4 0 0	31	33	1.974	1.973
3 3 1	6.2	11	1.812	1.810
4 2 0	2.6	1.5	1.767	1.765
4 2 2	40	37	1.613	1.611
5 1 1, 3 3 3	5.4	7.8	1.5190	1.5187
4 4 0	18	18	1.3945	1.3950
5 3 1	4.6	7.5	1.3325	1.3339
6 0 0, 4 4 2	1.1	0.5	1.3158	1.3152
6 2 0	15	15	1.2477	1.2477
5 3 3	1.5	2.7	1.2032	1.2034
6 2 2	0	0	—	1.1897
4 4 4	4.7	5.7	1.1392	1.1390
5 5 1, 7 1 1	2.2	4.1	1.1051	1.1050
6 4 0	0	0	—	1.0943
6 4 2	18	18	1.0544	1.0545
5 5 3, 7 3 1	3.0	5.2	1.0274	1.0274

$Fm3m$ space group with the observed integrated intensity, the ordering of Mg/Ir seems not to be complete for both high oxygen pressures samples (600 bar and 60 kbar) (Table 5). The B-site cation ordering is generally induced by a large difference in the oxidation states and the ionic radii. It is suggested that the size difference between the ionic radius of Mg^{II} ($r = 0.72$ Å) (45) and Ir^{VI} (0.50 Å $< r$ (Ir(VI)) < 0.55 Å) (37) could not be sufficient enough to induce a 1/1 cation ordering.

Magnetic Measurements

Magnetic susceptibility measurements were performed with an automatic DSM 8 type susceptometer in the range 4 to 800 K, with a magnetic field of 1.8 T. The equipment was calibrated using a single crystal of $Gd_2(SO_4)_3 \cdot 8H_2O$ for the low temperature region and Gd_2O_3 for the high temperature region.

After the correction of diamagnetic susceptibilities of the constitutient ions, the thermal variations of molar inverse magnetic susceptibilities ($\chi_M'^{-1} = f(T)$) are given in Figs. 4 and 5, respectively for $Sr_2CaIrO_{5.99}$ and $Sr_2MgIrO_{5.88}$, after the high oxygen pressure treatment at 600 bar (60 MPa) and 880°C. These compounds are antiferromagnetic with Néel temperatures close to 55 K for $Sr_2CaIrO_{5.99}$ and 80 K for $Sr_2MgIrO_{5.88}$. The evolution of the T_N values seems strongly correlated to the Ir–Ir distance in the perovskite lattice (Fig. 6).

The Curie constant of $Sr_2MgIrO_{5.88}$ in the paramagnetic temperature ($C_M = 1.20$) is less than that of $Sr_2CaIrO_{5.99}$ ($C_M = 1.66$), presumably due to the presence of Ir with a lower oxidation state. The deviation from linear plot in

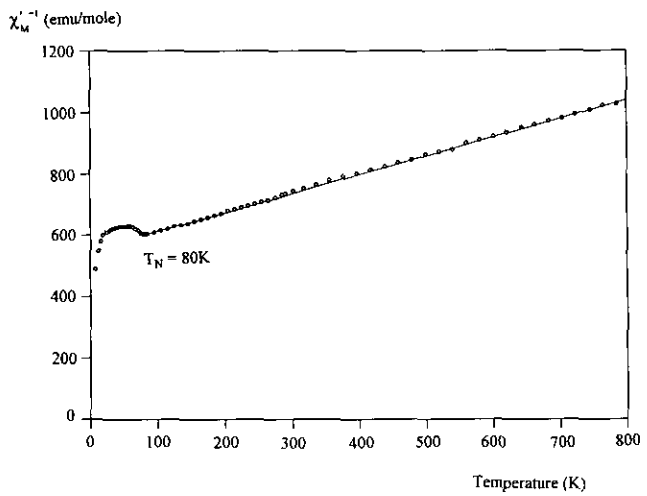

FIG. 4. Thermal variation of reciprocal molar magnetic susceptibility of Sr_2MgIrO_6.

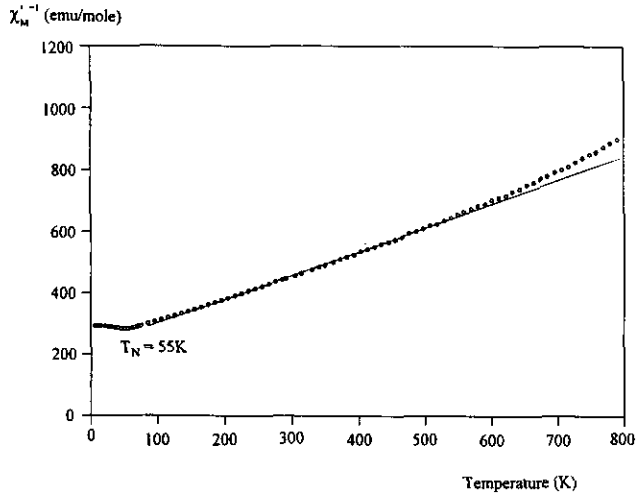

FIG. 5. Thermal variation of reciprocal molar magnetic susceptibility of Sr_2CaIrO_6.

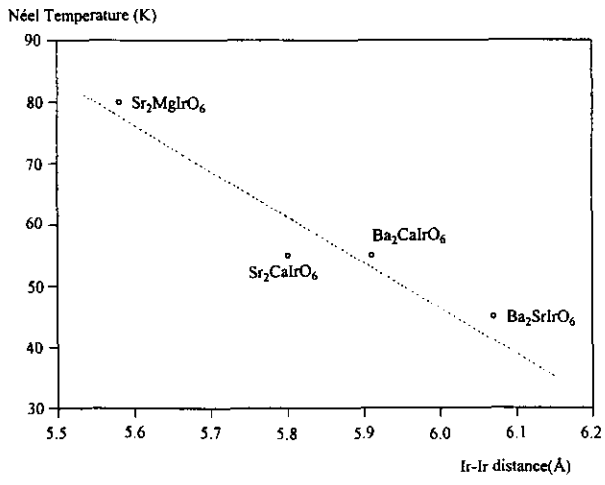

FIG. 6. Correlation between the distances of the nearest iridium ions and the Néel temperature in the prepared Ir(VI) perovskite oxides.

Sr_2CaIrO_6 above 500°C is attributed to a change of oxygen content as verified by use of the thermogravimetric analysis and X-ray diffraction data versus temperature.

The magnetic data for $Ba_2M'IrO_6$ (M' = Sr, Ca) and Sr_2MIrO_6 (M = Ca, Mg) are summarized in Table 6.

The d^3 electronic configuration, Ir(VI) characterized by a $^4A_{2g}$ term, is expected to lead to a smaller moment than that corresponding to the spin-only value, the only second-order orbital contribution being involved ($\mu_{eff} = \mu_{so}(1-4\lambda/10D_q)$ where μ_{so} is the spin only constant and λ is the spin-orbit coupling constant). The experimental magnetic moments approach the spin-only ones due to the local large crystal field energy corresponding to Ir(VI), the $4\lambda/10D_q$ term becoming small.

Electrical Measurement

Electrical conductivity was carried out on ceramics prepared from powder by the conventional four-probe method with silver paste contacts from room temperature down to 180 K (M = Mg) and 120 K (M = Ca) for the compounds prepared at 900°C, 600 bar (60 MPa).

Sr_2MIrO_6 (M = Ca, Mg) shows semiconducting behavior (Fig. 7). The calculated activation energies by the equation $\sigma = \sigma_0 \exp(-E_a/kT)$ for Sr_2MIrO_6 (M = Ca, Mg) are respectively close to 0.10 and 0.06 eV. Such small values could be due to the grain boundaries. At the same temperature a strong increase in the electrical conductivity is observed from M = Ca to Mg phase. The tendency is in agreement with the decrease in the cell volume suggesting a reduction of the electronic localization for the Ir(VI) t_{2g} electrons.

DISCUSSION

A high pressure oxygen treatment is necessary for the preparation of Sr_2MIrO_6 (M = Ca, Mg) which contain

TABLE 6
Magnetic Data and Distances between Iridium Ions for the Perovskite $A_2^{II}M^{II}Ir^{VI}O_6$ Prepared by High Oxygen Pressure of 600 bar (60 MPa) at 880°C[a]

Phase	C_M (emu · K/mole)[b]	μ_{eff} (μ_B)[c]	θ (K)[d]	T_N (K)	d(Ir–Ir) (Å)[e]
$Sr_2CaIrO_{5.99}$	1.66	3.66	−375	55	5.80
$Sr_2MgIrO_{5.88}$	1.20	3.11	−724	80	5.58
$Ba_2CaIrO_{6.00}$	1.89	3.90	−573	55	5.91
$Ba_2SrIrO_{5.88}$	1.64	3.64	−365	45	6.07

[a] The theoretical C_M and μ_{eff} values for spin-only contributions are respectively C_M = 1.875 and $\mu_{eff} = 3.89\mu_B$.

[b] C_M is the molar Curie constant calculated from the linear portion of the plot of χ'^{-1}_M vs T.

[c] Effective magnetic moment calculated from the equation $\mu_{eff} = 2.84\,(C_M)^{1/2}$ (μ_B)

[d] θ is the intercept on the temperature axis, extrapolated from the linear portion of the plot of χ'^{-1}_M vs T.

[e] d is the distance between nearest iridium ions in the ordered perovskite structure.

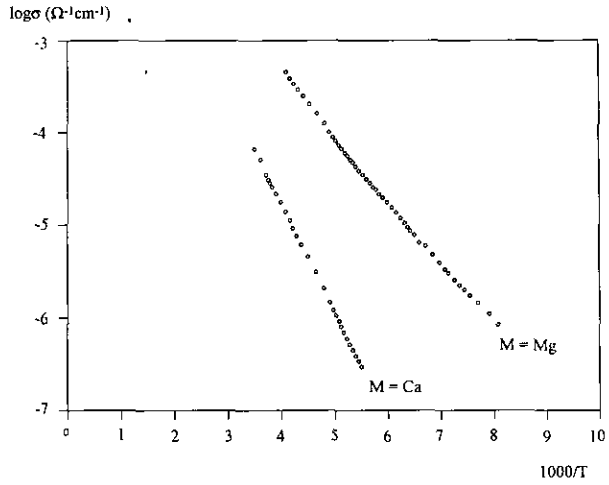

FIG. 7. Electrical conductivity vs reciprocal temperaure for Sr_2M IrO_6 (M = Ca, Mg).

Ir(VI), as shown by chemical titration and thermogravimetric analysis. Sr_2MIrO_6 (M = Ca, Mg) are more strongly influenced by oxygen pressure than the previously reported perovskite oxides of the type $Ba_2M'IrO_6$ (M' = Sr, Ca) (37). It is suggested that not only the strength of the competing bond M/M'–O, but also the acidity of 12-coordinated cations (Ba or Sr) can play an important role for the stabilization of iridium(VI).

Since the iridium perovskite oxides prepared in this study are a unique example of the stable Ir(VI)–O bond, it is very meaningful to calculate the Ir(VI)–O bond length. By use of Rietveld X-ray diffraction refinement, we have obtained bond lengths of 1.90, 1.95, and 1.90 Å for Ba_2SrIrO_6, Ba_2CaIrO_6, and Sr_2CaIrO_6, respectively. It can be suggested that the ionic radius of Ir(VI) in octahedral symmetry is close to 0.52 Å considering the average Ir–O bond length in these compounds (close to 1.92 Å) and six-coordinated oxygen radius of 1.40 Å (45). That is smaller than the ionic radius of Ir(V) (0.57 Å) (45). The ionic radius of Ir(VI) is not surprising due to the strong covalency of Ir(VI)–O resulting from the high oxidation state of iridium and the position of Ir (5d) in the periodic table.

In conclusion, the stabilization of Ir(VI) (d^3) is strongly correlated to the local crystal field energy mainly governed by the nature of the competing M–O bond. The $GdFeO_3$ structural distortion does not modify strongly the octahedal sites (40, 46). The high values of T_N for a super–super exchange interaction are consistant with the strong covalency of the Ir(VI)–O bond.

REFERENCES

1. B. L. Chamberland, *J. Less-Common Met.* **171,** 377 (1991).
2. J. Wilkens and H. K. Muller-Buschbaum, *Z. Anorg. Allg. Chem.* **592,** 79 (1991).
3. T. Siegrist and B. L. Chamberland, *J. Less-Common Met.* **170,** 93 (1991).
4. Ch. Lang and Hk. Muller-Buschbaum, *Monatsh. Chem.* **120,** 705 (1989).
5. H. U. Schaller, S. Kemmler-Sack, and A. Ehmann, *J. Less-Common Met.* **97,** 299 (1984).
6. B. L. Chamberland and S. Silvermane, *J. Less-Common Met.* **65,** P41 (1979).
7. W. D. Komer and D. J. Machin, *J. Less-Common Met.* **61,** 91 (1978).
8. P. L. Gai, A. J. Jacobson, and C. N. R. Rao, *Inorg. Chem.* **15,** 480 (1976).
9. A. W. Sleight, *Mater. Res. Bull.* **9,** 1177 (1974).
10. B. L. Chamberland and A. R. Philpotts, *J. Alloys Compounds* **182,** 355 (1992).
11. H. Schmalle, Ch. Gurtner, H. R. Oswald, and A. Reller, *Z. Kristallogr.* **191,** 239 (1990).
12. J. A. Kafalas and J. M. Longo, *J. Solid State Chem.* **4,** 55 (1972).
13. J. M. Longo, J. A. Kafalas, and R. J. Arnott, *J. Solid State Chem.* **3,** 174 (1971).
14. C. L. McDaniel and S. J. Schneider, *J. Res. Nat. Bur. Stand. A.* **75,** 185 (1971).
15. J. J. Randall and R. Ward, *J. Am. Chem. Soc.* **81,** 2629 (1959).
16. J. J. Randall, Jr. and L. Katz, *Acta Cystallogr.* **12,** 519 (1959).
17. J. J. Randall, Jr., L. Katz, and R. Ward, *J. Am. Chem. Soc.* **79,** 266 (1957).
18. R. F. Sarkozy, C. W. Moeller, and B. L. Chamberland, *J. Solid State Chem.* **9,** 242 (1974).
19. C. L. McDaniel and S. J. Schneider, *J. Solid State Chem.* **4,** 275 (1972).
20. J. A. Kafalas and J. M. Longo, *J. Solid State Chem.* **4,** 55 (1972).
21. V. D. Babel, W. Rudorff, and R. Tschopp, *Z. Anorg. Allg. Chem.* **347,** 282 (1966).
22. V. F. Rodi and D. Babel, *Z. Anorg. Allg. Chem.* **336,** 17 (1965).
23. K. Hayashi, G. Demazeau, M. Pouchard, and P. Hagenmuller, *Mater. Res. Bull.* **15,** 461 (1980).
24. K. Hayashi, G. Demazeau, and M. Pouchard, *C. R. Acad. Sci. Paris* **292,** 1433 (1981).
25. J. Darriet, G. Demazeau, and M. Pouchard, *Mater. Res. Bull.* **16,** 1013 (1981).
26. M. Walewski, B. Buffat, G. Demazeau, F. Wagner, M. Pouchard, and P. Hagenmuller, *Mater. Res. Bull.* **18,** 881 (1983).
27. P. Hagenmuller, (ed.) *in* "Preparative Methods in Solid State Chemistry" (J. B. Goodenough, J. A. Kafalas, and J. M. Longo, Eds.), Academic Press, New York, London, 1972.
28. Ch. Lang and Hk. Huller-Buschbaum, *J. Less-Common Met.* **161,** 1 (1990).
29. V. I. Thumm, U. Treiber, and S. Kemmler-Sack, *Z. Anorg. Allg. Chem.* **477,** 161 (1981).
30. I. Thumm, U. Treiber, and S. Kemmler-Sack, *J. Solid State Chem.* **35,** 156 (1980).
31. R. C. Byrne and C. W. Moeller, *J. Solid State Chem.* **2,** 228 (1970).
32. J. G. Dickson, L. Katz, and R. Ward, *J. Am. Chem. Soc.* **83,** 3026 (1961).
33. Ch. Lang and Hk. Muller-Buschbaum, *Z. Anorg. Allg. Chem.* **574,** 169 (1989).
34. M. Drillon, G. Pourroy, and J. Darriet, *Chem. Phys.* **88,** 27 (1984).
35. V. U. Treiber, S. Kemmler-Sack, and A. Ehmann, *Z. Anorg. Allg. Chem.* **487,** 189 (1982).
36. G. Demazeau, D. Y. Jung, J. P. Sanchez, E. Colineau, A. Blaise, and L. Fournes, *Solid State Commun.* **85,** 479 (1993).
37. D. Y. Jung, P. Gravereau, and G. Demazeau, *Eur. J. Solid State Inorg. Chem.* **30,** 1025 (1993).
38. R. B. Roof, "Los Alamos Sci. Laboratory *Report* 1976, LA-6495-MS," Los Alamos, NM; (*Chem. Abstr.* **86,** 19,8367 (1977)).

39. G. Demazeau, Thesis, University of Bordeaux 1, 1973.
40. S. Geller, *J. Chem. Phys.* **24,** 1236 (1956).
41. P. D. Battle and W. J. Macklin, *J. Solid State Chem.* **52,** 138 (1984).
42. P. D. Battle, J. B. Goodenough, and R. Price, *J. Solid State Chem.* **46,** 234 (1983).
43. H. M. Rietveld, *J. Appl. Crystallogr.* **2,** 65 (1969).
44. D. B. Wiles and R. A. Young, *J. Appl. Crystallogr.* **14,** 149 (1981).
45. R. D. Shannon, *Acta Crystallogr. Sect A* **32,** 751 (1976).
46. M. Marezio, J. P. Pemeika, and P. D. Dernier, *Acta Crystallogr. Sect. B* **26,** 2008 (1970).